Vibration of fiber reinforced anisotropic composite plates with nanofiber reinforced matrices

C. C. Chamis & P. L. N. Murthy
National Aeronautics and Space Administration Glenn Research Center, Cleveland, Ohio, USA

Abstract

Anisotropic composite plates were evaluated with nanofiber reinforced matrices (NFRM). The nanofiber reinforcement volumes ratio in the matrix was 0.01. The plate dimensions were 20 by 10 by 1.0 in. (508 by 254 by 25.4 mm). Seven different loading condition cases were evaluated: three for uniaxial loading, three for pairs of combined loading, and one with three combined loadings. The anisotropy arose from the unidirectional plates having been at 30° from the structural axis. The anisotropy had a full 6 by 6 rigidities matrix which were satisfied and solved by a Galerkin buckling algorithm. The buckling results showed that the NFRM plates buckled at about twice those with conventional matrix.
Keywords: combined vibration frequencies, buckling influence, plate vibration at different or orientation angles, comparisons with conventional matrix.

1 Introduction

Considerable research activities in nanocomposites have been actively pursued recently. One aspect of this research is on nanofiber reinforced matrices (NFRM) which can subsequently be used as matrices in conventional reinforced fiber composites [1–3]. Reference [1] includes pertinent references to that date. Reference [3] includes additional references to 2009. However, to date, the vibration of composite plates with NFRM has not been investigated yet. This is the objective of the present paper, to use commercial composites with NFRM loaded at 30° from the material axis (Fig. 1) for seven different load cases shown in Table 6 for uniaxial and combined load conditions.

WIT Transactions on The Built Environment, Vol 124,
www.witpress.com, ISSN 1743-3509 (on-line)
doi:10.2495/HPSM120191

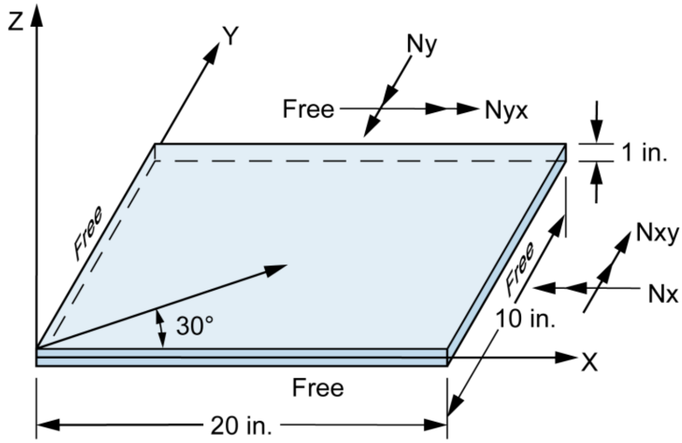

Figure 1: Anisotropic plate schematic.

The plate is evaluated with fiber composite in the NFRM that is an AS/IMHS (AS graphite fiber/intermediate modulus high strength matrix) for all the loading cases. Because the 30° off-axis composite has a full 6×6 bending stiffness matrix, a Galerkin algorithm is used to evaluate the vibration frequencies. The bending stiffness required for the vibration frequencies of off-axis loaded anisotropic composite were generated by the in-house integrated computer code in composite mechanics. The results with and without the NFRM show about 60 percent increase in the vibration frequencies for all loading cases with only 1 percent of nanofiber reinforced matrix. Results are presented for the frequency mode and its corresponding numerical value for each loading case. The graphical results shown will be for the type of loading condition, the 3-D vibration frequencies mode shape, a counter plot of the buckling factor mode and a 3-D plot of the buckling. One interesting result is that the shear frequency factor requires a tiny small loading in one or both structural axes to enhance the convergence.

2 Background theory

The theory was developed when the first author was a graduate student at Case Western Reserve University and it is described in [4]. The application to the anisotropic plates was performed when he started working at NASA Lewis Research Center (now Glenn Research Center) [2]. The programming details source code and several sample cases are in the appendices of [5]. The brief description of the theoretical background is from [5] also. The underlying theory for vibration frequencies of anisotropic plates is described in [4, 5] with pertinent discussions in [6–8]. Briefly, this theory consists of expressing the potential energy of plate anisotropic composite in terms of displacement variables. Taking

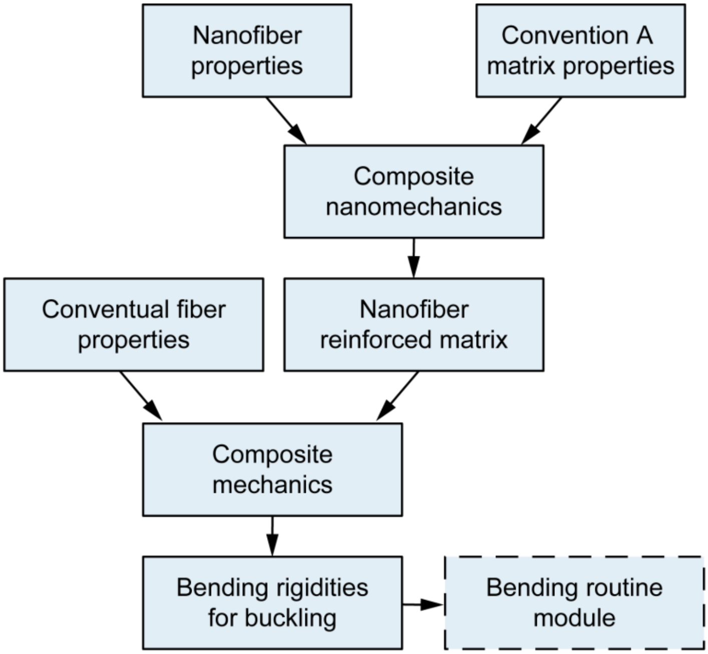

Figure 2: Simulation of nanofiber reinforced matrix schematic.

the variation of the potential energy function yields the field equation and the corresponding boundary conditions. The resulting system is then solved by the assumed mode technique in conjunction with the Galerkin method (Fig. 2).

The equation resulting after the variation of the energy function is

$$\begin{aligned}
&\int_0^a\int_0^b \Big[D_{11}w,_{xxxx} + 2\left(D_{12}+2D_{33}\right)w,_{xxyy} + D_{22}w,_{yyyy} + 4D_{13}w,_{xyxx} \\
&\qquad + 4D_{23}w,_{xyyy} - \left(\bar{N}_X w,_{xx} + 2\bar{N}_{xy} w,_{xy} + N_y w,_{yy}\right)\Big]\,\delta w\, dy\, dx \\
&\qquad + \int_0^b \left(D_{11}w,_{xx} + D_{12}w,_{yy} + 2D_{13}w,_{xy}\right|_0^a \delta w,_x\, dy \\
&\qquad + \int_0^a \left(D_{21}w,_{xx} + D_{22}w,_{yy} + 2D_{23}w,_{xy}\right|_0^b \delta w,_y\, dx = 0
\end{aligned} \tag{1}$$

(The notation is defined in Appendix A of [2].) The area integral represents the field equation, and the line integrals represent the boundary conditions.

The assumed vibration mode described in [2] is represented by a Fourier double sine series. This mode satisfies the imposed boundary conditions, but it does not satisfy the natural boundary conditions if the material and structural axes do not coincide. However, the mode is forced to satisfy the natural boundary conditions approximately through the Galerkin method as discussed in [2]. Substituting the assumed mode in Equation (1), applying the Galerkin method, and carrying out the algebra result in a set of linear equations

$$[M]\,\ddot{w}+[K]\,\{w\}=\lambda\,[L]\,\{w\} \tag{2}$$

where M is the mass matrix, K is the stiffness matrix, λ is the eigenvalue [L] is the loading matrix and {w} is the displacement vector which represent the eigenvalue problem of the plate. This system is coupled for either a combination of shear and normal loads and/or noncoincident material and structural axes. The eigenvalue problem is solved by using the Power method, which is a highly effective iterative numerical technique in seeking the largest eigenvalue of the system. The indicial equations which were used to generate this system and the Power method are given in Appendix B of [5] in outline form. The source code has been reprogrammed by Dr. Murthy in Matlab.

3 Result and discussion

The frequency results presented subsequently are from the Matlab reprogrammed. There are two portions to the results: (1) is the simulation of the NFRM which is performed by a composite mechanics code ICAN/JAVA in order to obtain the nanofiber reinforcement in the matrix and (2) using the NFRM in the mechanics computer code again to simulate the effects of the reinforced matrix in the dynamic behavior of the composite plate for different combination of loads. The nanofiber reinforced matrix (NFRM) is simulated by using the nanofiber properties shown in Table 1 in an intermediate modules high strength matrix in Table 2 assuming a quasi isotropic fiber arrangement.

The properties of this lay-up arrangement are shown in Table 3. Next, the conventional fiber in Table 4 was used with the NFRM to obtain the bending rigidities shown in Table 5.

The composite plate shown in Figure 1 was selected for the dynamic evaluation. The fiber reinforcement was 0.6 volume ration in a NFRM. The bending rigidities shown in Table 5 were transformed to 30° from the structural x-axis to obtain the anisotropic composite plate. The transformed rigidities were input into the frequency routine with the plate geometry (20×10×1.0) length, width, thickness and the results were obtained for seven different cases of combined in plane loads. For convenience all the inplane loads were assumed to be of equal magnitude. Two different frequency results are shown for conventional matrix Table 6 and for NFRM Table 7.

www.witpress.com, ISSN 1743-3509 (on-line)

Table 1: Nanofiber (trial fiber) [Trial fiber modulus 123M for single fiber 3-D stress analysis.].

Description	Symbol	Value	Value in SI units
Number of fibers per end	Nf	100.0	100
Filament equivalent diameter	df	4.0×10^{-10} in.	1.016×10^{-8} mm.
Weight density	Rhof	0.06 lb/in.^{3}	1.661×10^{-6} kg/mm^3
Normal moduli (11)	Ef11	1.0×10^{9} psi	689.5×10^{10} Pa
Normal moduli (22)	Ef22	41.0×10^{7} psi	282.7×10^{10} Pa
Poisson's ratio (12)	Nuf12	0.2 non-dim.	0.2 non-dim.
Poisson's ratio (23)	Nuf23	0.35 non-dim.	0.35 non-dim.
Shear moduli (12)	Gf12	2.0×10^{7} psi	13.79×10^{10} Pa
Shear moduli (23)	Gf23	1.5×10^{7} psi	10.34×10^{10} Pa
Thermal expansion coefficient (11)	Alfaf11	-6.0×10^{-8} in./in./°F	-10.8×10^{-8} /°C
Thermal expansion coefficient (22)	Alfaf22	6.0×10^{-6} in./in./°F	10.8×10^{-6} /°C
Heat conductivity (11)	Kf11	400.0 BTU/hr/in./°F	8.3075 W/mm/°C
Heat conductivity (12)	Kf12	40.0 BTU/hr/in./°F	0.83075 W/mm/°C
Heat capacity	Cf	0.17 BTU/lb/°F	712.3 J/kg/°C
Dielectric strength (11)	Kef11	0.0 V/in.	0.0 V/mm
Dielectric strength (22)	Kef22	0.0 V/in.	0.0 V/mm
Dielectric constant (11)	Gammaf11	0.0 in./V	0.0 mm/V
Dielectric constant (22)	Gammaf22	0.0 in./V	0.0 mm/V
Capacitance	Cef	0.0 V	0.0 V
Resistivity	Ref	0.0 Ω-in.	0.0 Ω-mm
Tensile strength	SfT	1000000.0 psi	6895×10^{6} Pa
Compressive strength	SfC	900000.0 psi	6205×10^{6} Pa
Shear strength	SfS	500000.0 psi	3447×10^{6} Pa
Normal damping capacity (11)	psi11f	0.03 %Energy	0.03 %Energy
Normal damping capacity (12)	psi22f	0.4 %Energy	0.4 %Energy
Shear damping capacity (12)	psi12f	0.4 %Energy	0.4 %Energy
Shear damping capacity (23)	psi23f	0.8 %Energy	0.8 %Energy
Melting temperature	TMf	6000.0 °F	3315.6 °C

Table 2: Conventional matrix (IMHS) [Intermediate modulus 123M for single fiber 3-D stress analysis.].

Description	Symbol	Value	Value in SI units
Weight density	Rhom	0.044 lb/in.^{3}	1.218×10^{-6} kg/mm^3
Normal modulus	Em	10000000psi	68.94 GPa
Poisson's ratio	Num	0.35 non-dim.	0.35 non-dim.
Thermal expansion coefficient	Alfa m	3.6×10^{-5} in./in./°F	6.48×10^{-5}/°C
Heat conductivity	Km	0.008681 BTU/hr/in./°F	1.803×10^{-4}W/mm/°C
Heat capacity	Cm	0.25 BTU/lb/°F	1048 J/kg/°C
Dielectric strength	Kem	0.0 V/in.	0.0 V/mm
Dielectric constant	Gammam	0.0 in./V	0.0 V/mm
Capacitance	Cem	0.0 V	0.0 V
Resistivity	Rem	0.0 Ω-in.	0.0 Ω-mm
Moisture expansion coefficient	Betam	0.0033 in./in./%Moisture	0.0033 /%Moisture
Diffusivity	Dm	2.16×10^{-7} in.^{2}/hr	1.394×10^{-4} mm^2/hr
Saturation	Mm	0.0 %Moisture	0.0 %Moisture
Tensile strength	SmT	15000.0 psi	103.4 MPa
Compressive strength	SmC	35000.0 psi	241.3 MPa
Shear strength	SmS	13000.0 psi	89.63 MPa
Allowable tensile strain	eps mT	0.02 in./in.	0.02 mm/mm
Allowable compr. strain	eps mC	0.05 in./in.	0.05 mm/mm
Allowable shear strain	eps mS	0.035 in./in.	0.035 mm/mm
Allowable torsional strain	eps mTOR	0.035 in./in.	0.035 mm/mm
Normal damping capacity	psiNm	6.6 %Energy	6.6 %Energy
Shear damping capacity	psiSm	6.9 %Energy	6.9 %Energy
Void heat conductivity	Kv	0.225 BTU/hr/in./°F	4.673×10^{-3} W/mm/°C
Glass transition temperature	Tgdr	420.0 °F	215.6 °C
Melting temperature	TMm	0.0 °F	–17.78 °C

Table 3: NanoFiber reinforced matrix (NFRM—0.01 fiber reinforcement).

Description	Symbol	Value	Value in SI units
Weight density	Rhom	0.047 lb/in.^{3}	1.301×10^{-6} kg/mm^3
Normal modulus	Em	6.774×10^7 psi	467.1 GPa
Poisson's ratio	Num	0.3323 non-dim.	0.3323 non-dim
Thermal expansion coefficient	Alfa m	5.6×10^{-9} in./in./°F	10.08×10^{-9}/°C
Heat conductivity	Km	444.0 BTU/hr/in./°F	9.221 W/mm/°C
Heat capacity	Cm	0.227 BTU/lb/°F	951.1 J/kg/°C
Dielectric strength	Kem	0.0 V/in.	0.0 V/mm
Dielectric constant	Gammam	0.0 in./V	0.0 V/mm
Capacitance	Cem	0.0 V	0.0 V
Resistivity	Rem	0.0 Ω-in.	0.0 Ω-mm
Moisture expansion coefficient	Betam	5.5×10^{-11} in./in./%Moisture	5.5×10^{-11} /%Moisture
Diffusivity	Dm	5.4×10^{-11} in.^{2}/hr	3.484×10^{-8} mm^2/hr
Saturation	Mm	0.0 %Moisture	0.0 %Moisture
Tensile strength	SmT	800000.0 psi	5.516 GPa
Compressive strength	SmC	600000.0 psi	4.137 GPa
Shear strength	SmS	400000.0 psi	2.758 GPa
Allowable tensile strain	eps mT	0.0070 in./in.	0.0070 mm/mm
Allowable compr. strain	eps mC	0.0060 in./in.	0.0060 mm/mm
Allowable shear strain	eps mS	0.0040 in./in.	0.0040 mm/mm
Allowable torsional strain	eps mTOR	0.0040 in./in.	0.0040 mm/mm
Normal damping capacity	psiNm	0.4 %Energy	0.4 %Energy
Shear damping capacity	psiSm	0.4 %Energy	0.4 %Energy
Void heat conductivity	Kv	0.225 BTU/hr/in./°F	4.673×10^{-3} W/mm/°C
Glass transition temperature	Tgdr	420.0 °F	215.6 °C
Melting temperature	TMm	550.0 °F	287.8 °C

Table 4: Conventional fiber (AS00).

Description	Symbol	Value	Value in SI units
Number of fibers per end	Nf	10000.0	10000.0
Filament equivalent diameter	df	3.0×10^{-4} in.	76.2×10^{-4} mm.
Weight density	Rhof	0.063 lb/in.^{3}	1.744×10^{-6} kg/mm^3
Normal moduli (11)	Ef11	3.2×10^7 psi	22.06×10^{10} Pa
Normal moduli (22)	Ef22	2000000.0 psi	13.79 GPa
Poisson's ratio (12)	Nuf12	0.2 non-dim.	0.2 non-dim.
Poisson's ratio (23)	Nuf23	0.25 non-dim.	0.25 non-dim.
Shear moduli (12)	Gf12	2000000.0 psi	13.79 G Pa
Shear moduli (23)	Gf23	1000000.0 psi	6.895 GPa
Thermal expansion coefficient (11)	Alfaf11	5.5×10^{-7} in./in./°F	9.9×10^{-7}/°C
Thermal expansion coefficient (22)	Alfaf22	5.5×10^{-4} in./in./°F	9.9×10^{-4}/°C
Heat conductivity (11)	Kf11	4.03 BTU/hr/in./°F	0.08370 W/mm/°C
Heat conductivity (12)	Kf12	0.403 BTU/hr/in./°F	0.008370 W/mm/°C
Heat capacity	Cf	0.17 BTU/lb/°F	712.3 J/kg/°C
Dielectric strength (11)	Kef11	0.0 V/in.	0.0 V/mm
Dielectric strength (22)	Kef22	0.0 V/in.	0.0 V/mm
Dielectric constant (11)	Gammaf11	0.0 in./V	0.0 mm/V
Dielectric constant (22)	Gammaf22	0.0 in./V	0.0 mm/V
Capacitance	Cef	0.0 V	0.0 V
Resistivity	Ref	0.0 Ω-in.	0.0 Ω-mm
Tensile strength	SfT	400000.0 psi	2.758 GPa
Compressive strength	SfC	350000.0 psi	2.413 GPa
Shear strength	SfS	250000.0 psi	1.724 GPa
Normal damping capacity (11)	psi11f	0.05 %Energy	0.05 %Energy
normal damping capacity (12)	psi22f	0.25 %Energy	0.25 %Energy
Shear damping capacity (12)	psi12f	0.35 %Energy	0.35 %Energy
Shear damping capacity (23)	psi23f	0.5 %Energy	0.5 %Energy
Melting temperature	TMf	6000.0 °F	3315.6 °C

Table 5: Bending regidities of unidirectional composite for buckling analysis.

θ	D_{11}	D_{12}	D_{13}	D_{22}	D_{23}	D_{33}	Comment
0	3.87 + 6	5.41 + 4	0	2.14 + 4	0	2.10 + 4	With NFRM; $k_f = 0.01$
0	1.62 + 6	2.60 + 5	0	9.98 + 4	0	5.19 + 4	Without NFRM
kPa	27.10 + 6	6.08 + 4	0	14.94 + 5	0	14.66 + 5	
kPa	11.31 + 6	18.15 + 5	0	69.60 + 4	0	36.23 + 4	

Table 6: Buckling factor results on anisotropic composite plates with conventional matrix.

Load conditions in vibration frequencies			
√	0	0	–1793
0	√	0	–529
0	0	√	–1023
√	√	0	–422
√	0	√	–708
0	√	√	–383
√	√	√	–323

Table 7: Buckling factor results of anisotropic composite plates with NFRM.

Load conditions in vibration frequencies			
√	0	0	–3673
0	√	0	–1097
0	0	√	–2220
√	√	0	–875
√	0	√	–1523
0	√	√	–808
√	√	√	–680

The vibration frequency evaluations indicated in each table with a check mark. Note that the structural axis has only one check mark in the first column. The y axis has one check mark in the second column. The x-y loading has a check mark in the third column combined load cases leave check marks in the appropriate column to indicate the combined loading. Comparing the frequency results of the two tables it is seen that the plates with the NFRM is about 60-percent of the conventional matrix.

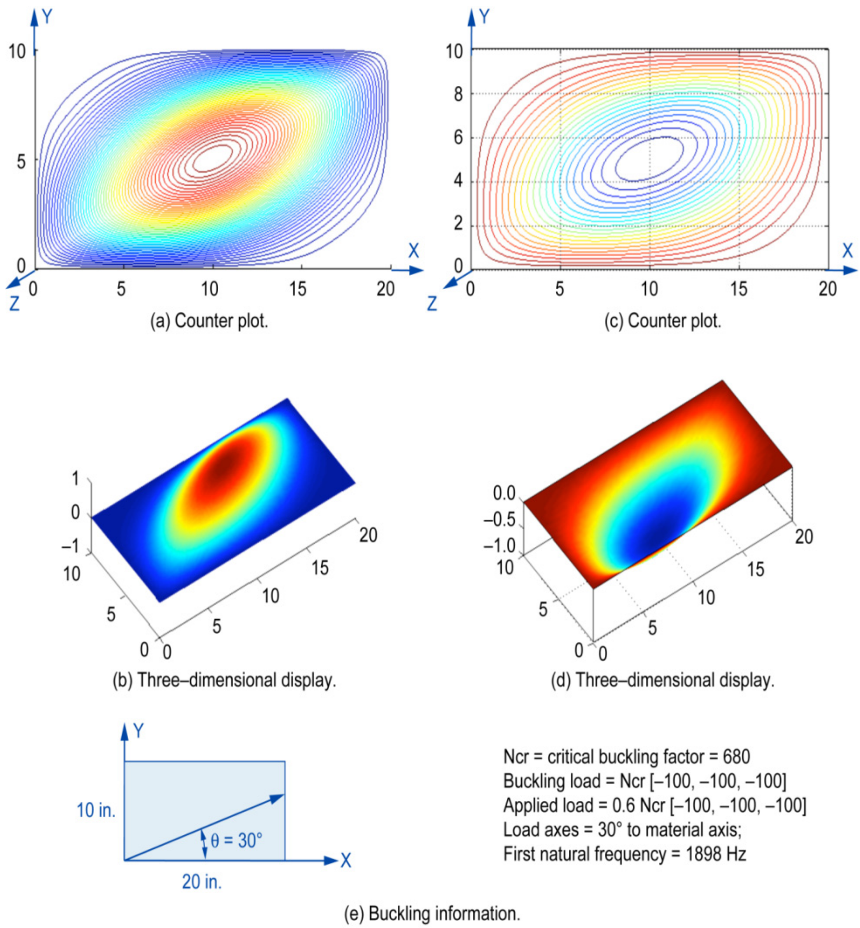

Figure 3: Buckling factor and first frequency vibration mode.

4 Vibration frequencies mode shapes

The vibration frequencies mode shapes of anisotropic plates is very interesting. In this evaluation vibration frequencies mode shapes were evaluated for each loading case that means there are seven charts of vibration frequencies mode shapes. Each chart has four parts in it. The top is a counter part of the modal shapes. The center is a 3-D view of the buckling factor and the vibration frequencies mode shape. The lower part shows the angle of the anisotropy.

Figure 3 is the load factor and frequency mode shape of x, y, and xy -axes and shear load. As was the case previously, the counter plot show symmetry about the material axis. The frequency converged in 8 iterations with a value of load factor 680 lb (30.25 kN) and the frequency is 1898 Hz.

www.witpress.com, ISSN 1743-3509 (on-line)

Figure 3 depicts the load factor and frequency mode shape of combined loads x, y, and xy. The load factor is 680 lb (30.25 kN) and the frequency is 1898 Hz.

Figure 4 shows the highly nonlinear effects of increasing load in the natural frequencies reaching zero at some load which corresponds to the buckling load. Note that the 45° curve reaches "zero" before the 60° curve. It also shows that at higher ages (>45°) the frequencies reach "zero" progressively.

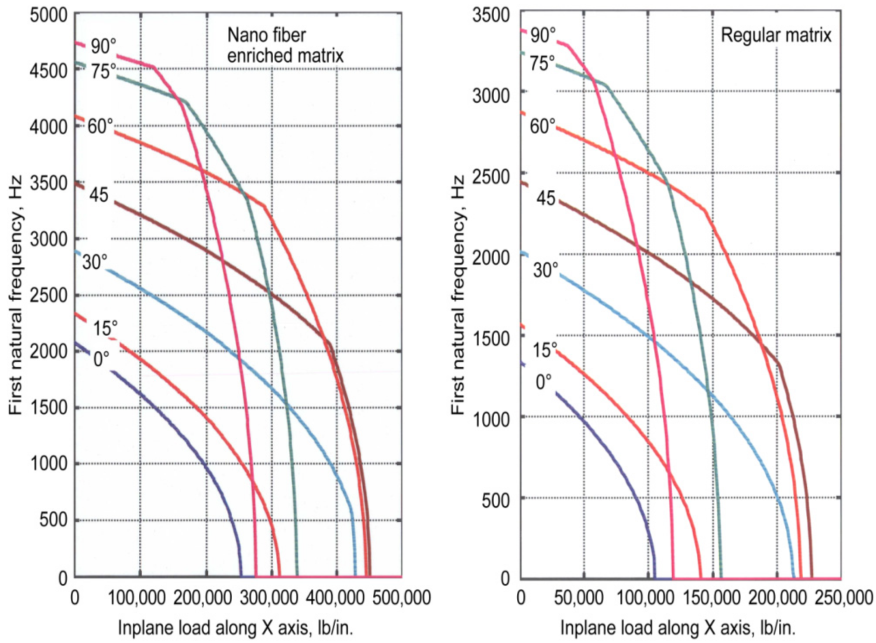

Figure 4: Increasing load effects on anisotropic frequencies.

5 Concluding remarks

The concluding remarks of frequency response of anisotropic composite plates with NFRM are as follows. The nanofiber reinforcement has a major effect in the vibration frequencies. All the cases investigated for combined loads showed the same about 60 percent benefit compared to conventional matrix. All vibration frequencies of the mode shape are single. All vibration frequencies mode counter plot showed symmetry about the matrix axis except the first case which showed symmetry about 45° to the structural x-axis. The shear loading only case required a small load in the two other orthogonal axes to expedite convergence. All vibration frequencies converged between 6 and 8 iterations. The frequency algorithm is very effective and its convergence is efficient. The simulation of the nanofiber reinforced matrix is also an effective means to obtain the influence of nanofibers in a matrix first and then combine the NFRF with the conventional fibers for other structure evaluation loading. The loading has severe effects on the frequency. All frequencies decrease nonlinearly with increasing load reaching “zero” at higher loads <45° and the “zero” load decreases at loads >4°. Decrease nonlinearly with increasing orientation angle.

6 Conversion factors

Inch = 2.54 cm
Weight density lb/in^3 = 0.02kg/cm^3
Psi = ~7 Pa
Thermal Expansion Coefficient in/in/^{0}F = 0.56cm/cm/$^{\circ\circ}$C
Thermal conductivity btu/hr/ft/^{0}F = 1.731W/mK
Specific heat Btu/lb/^{0}F – 4188J/kg K

References

[1] Gates, T.S. *et al*. Computational materials: Multi-scale modeling and simulation of nanostructured materials. Composite Science 65, pp. 2416 - 2434, 2005.
[2] Chamis, C. C. *et al.* Composite Nanomechanics: A Mechanistic Approach. NASA TM—2007-214673, 2007.
[3] Ansari, M.N.M., *et al.* Effect of Multi-walled Carbon Nanotubes on Mechanical Properties of Feldspar filled Polypropylene Composites. Reinforced Plastics and Composites, Vol.28, No. 20, 2009.
[4] Chamis, C.C.: Buckling of Anisotropic Composite Plates. J. Structural Div., ASCE, vol. 95, no. ST10, Oct. 1969, pp. 2119– 2139.
[5] Chamis, C.C.: Buckling Loads of Boron/Aluminum and Graphite/Resis Fiber Composite Anisotropic Plates. NASA TND 6572, December 1971.
[6] Wang, James T.-S.: On the Solution of Plates of Composite Materials. J. Composite Mat., vol. 3, July 1969, pp. 590–592.
[7] Hsu, T.M.: Buckling of Anisotropic Plates, Discussion J. Structural Div., Am. Soc. Civil Eng., vol. 96, no. ST7, July 970, pp. 1604.
[8] Chamis, C.C.: Buckling of Anisotropic Plates, Closure and Errata. Structural Div., Am. Soc. Civil Eng., vol. 97, no. ST3, Mar. 1971, pp. 960.